Journal of Materials Science & Technology 112 (2022) 195–201

Contents lists available at ScienceDirect

Journal of Materials Science & Technology

journal homepage: www.elsevier.com/locate/jmst

Excellent strength-ductility synergy properties of gradient nano-grained structural CrCoNi medium-entropy alloy

Wenjie Lu[a,b], Xian Luo[a,*], Dou Ning[a], Miao Wang[c], Chao Yang[a], Miaoquan Li[a], Yanqing Yang[a,b,*], Pengtao Li[a], Bin Huang[a]

[a] State Key Laboratory of Solidification Processing, Northwestern Polytechnical University, Xi'an 710072, China
[b] Langu Institute for Materials Analysis Co. Ltd, Weihai 264207, China
[c] School of Physics and Optoelectronic Engineering, Yangtze University, Jingzhou 434023, China

ARTICLE INFO

Article history:
Received 22 July 2021
Revised 7 September 2021
Accepted 8 September 2021
Available online 26 December 2021

Key words:
Medium-entropy alloy
Gradient nano-grained structure
High energy shot peening
Hetero-deformation induced hardening
Strength-ductility synergy

ABSTRACT

Tailoring heterogeneities could bring out excellent strength-ductility synergy properties. A gradient nano-grained (GNG) structure, i.e. grain size range from nanometer (~50 nm) at topest surface layer to micrometer (~1.3 μm) at center layer, was successfully introduced into CrCoNi medium-entropy alloy (MEA) by means of high energy shot peening in this work. Experimental results demonstrated that this GNG CrCoNi MEA shows excellent strength and ductility combination properties, exhibiting high yield strength and ultimate tensile strength of ~1215 MPa and ~1524 MPa, respectively, while remaining a good ductility of ~23.0%. The extraordinary hetero-deformation induced (HDI) hardening origins from heterogeneous structure, i. e. GNG structure, which contributes to the majority strength enhancement. Dynamical reinforced heterogeneous structure during tension process results in the enhanced HDI hardening effect, which facilitates excellent ductility and strain hardening capacity at high-level strength. Our work provide not only a feasible and effective way to strengthen the CrCoNi MEA, and other low stacking faults energy (SFE) materials, but also an useful insight to understanding HDI hardening in heterogeneous structure.

1. Introduction

As potential structural materials, face-centered cubic (FCC) type high/medium-entropy alloys (HEAs/MEAs) attracted more and more attentions [1–5], due to their many promising functional properties, e.g. excellent damage-tolerance [6,7], high wear and corrosion resistance [8–10], good irradiation resistance [11,12], as well as extraordinary cryogenic temperature performance [13,14], which make them strong candidate for engineering application. However, the obvious strength-ductility dilemma tradeoff in those FCC HEAs/MEAs [6,15,16], which exhibit relative low yield strength at room temperature in contrast with their excellent ductility, offer strong baulks for their application in structural engineering. Therefore, an appropriate design is highly demanded for FCC type HEAs/MEAs to obtain a superior combination of high strength and good ductility.

Traditional grain-boundary hardening [15,17,18] and precipitation hardening [13,19-22] could result in promising strengthening efficacies in HEAs/MEAs, nevertheless strength enhancement is accompanied by a high ductility sacrifice. Recent researches indicate that tailoring heterogeneities in metals and alloys could effectively bring out hetero-deformation inducing (HDI) hardening, which result in excellent strength-ductility synergy properties [23–30]. Wu et al. reported a three-level heterogeneous grain structure CrCoNi MEA with grain size spanning the nanometer to micrometer range through cold rolling (CR) and partial recrystallization annealing processes [27], which exhibited high a yield strength of above 1 GPa meanwhile remained an excellent uniform stain of ~22%. Fang et al. constructed an gradient nano-grained (GNG) structure in copper through a surface mechanical grinding treatment (SMGT) [29], which demonstrated superior strength-ductility synergy properties in comparison with the nano-grained (NG)/ coarse-grained (CG) copper. Inspired by the above strategy, tailoring structure heterogeneities, i.e. leading into HDI hardening, should be an interesting and effective way to obtain strength and ductility combination properties in FCC type HEAs/MEAs.

In present work, we chose the FCC type CrCoNi MEA as base material for HDI hardening, because of its high work hardenability and excellent ductility [7,16]. We successfully constructed a GNG

* Corresponding authors.
E-mail addresses: luoxian@nwpu.edu.cn (X. Luo), yqyang@nwpu.edu.cn (Y. Yang).

https://doi.org/10.1016/j.jmst.2021.09.058
1005-0302/

structure by means of high energy shot peening (HESP) in CG CrCoNi MEA. Experiment results indicate constructing GNG structure brings out superior strength and ductility synergy properties. The reasons for superb mechanical properties of this GNG structure are systematically investigated. Our work will not only prove that constructing GNG structure should be a feasible and effective way to deal with the strength and ductility tradeoff problem in FCC MEAs/HEAs, but also provide a useful insight of HDI hardening in heterogeneous structure.

2. Experimental procedure

The equimolar CrCoNi MEA was produced by arc-melting a mixture of pure metals of Cr, Co and Ni (purity >99.95 wt.%) in a Ti-gettered high-purity argon atmosphere, remelted at least four times. The ingot was drop-casted into a copper mold with a dimension of $10 \times 10 \times 50 mm^3$, then subsequently homogenized at 1473 K for 10 h. The as-homogenized ingots were cold rolled with a total thickness reduction of 80%, subsequently annealed at 973 K for 1 h and followed by water quenching. The annealed sheet was then processed by HESP treatment for both top and bottom surfaces at room temperature in a LSSKPWJ1512P-15 CNC shot blasting machine. During HESP, the ASH 230 cast steel shots with a diameter of 0.6 mm were violently accelerated at an air pressure of 0.25 MPa pressure for 15 min, and the peeing distance of 300 mm, working angle of 90° and the mass flow rate of 10 kg/min were adopted.

Rectangular dog-bone-shaped tensile specimens with a gage length of 12.5 mm, a gage width of 4 mm were fabricated by electrodischarge machining took from the HESP treated plate for tensile tests. The uniaxial tensile tests and loading-unloading-reloading (LUR) tests were performed at an engineering strain rate of $1 \times 10^{-3} s^{-1}$ in an INSTRON 3382 material testing machine at room temperature. Two samples for each condition were tested to make sure the data reproducibility.

The microstructure investigations were examined by the electron backscattering diffraction (EBSD, Oxford Instruments AZtecHKL) in a Zeiss Supra55 operating equipped with field emission gun electron source (FEG). Before EBSD investigation, samples were prepared using careful mechanical polishing followed by electropolishing using a solution of 10% perchloric acid and 90% ethanol with a direct voltage of 20 V at the temperature of −40 °C. Samples before and after tensile test for transmission electron microscopy (TEM) observations were cut by electrodischarge machining, then mechanically polished to a thickness of 50 μm, and then ion-beam thinning at a cryogenic state of 100 K. The topmost layer of sample for TEM observation was cut by gallium focused-ion-beam (FIB) with a FIB-SEM dual-beam system (Layra 3, Tescan). All those thin foils were observed by a Talos F200s TEM operating at 200 keV.

3. Results and discussion

3.1. Formation of gng structure in crconi mea

Fig. 1 shows the EBSD investigation of CG CrCoNi MEA subjected to CR and 973 K/1 h annealing treatments. The inverse pole figure (IPF) of Fig. 1(a) reveals an equiaxed grains structure with non-uniform grain sizes (see Fig. 1(b)), and the average grain size is ~1.3 μm (including twin boundaries) determined by a linear intercept method. High density thermal twins were detected in this CG MEA, as shown in Fig. 1(a) and (c), which attributed to the low stacking faults energy(SFE) of CrCoNi MEA, 22 ± 4 mJ/m^2 [16].

Fig. 2 shows the microstructure ecolutions of CG CrCoNi MEA sample after HESP treatment. Fig. 2(a-c) exhibits representative TEM bright-field (BF) at topmost surface, ~100 μm-deep layer and center layer, respectively. It can be clearly seen that, after HESP treatment, the topmost layer is composed of nanosize grains (NGs) with random orientations, as shown in Fig. 2(a), revealing an average grain size of ~50 nm. While at 100 μm-deep layer, the average grain size increase to ~300 nm, see in Fig. 2(b), wherein numerous deformation twins (DTs) divide the coarse grains to facilitate the formation of ultrafine grained (UFG) structure. TEM investigation indicates that a gradual grain size structure existed along the depth from topmost surface to ~350 μm-deep, i.e. forming a ~350 μm thickness GNG layer. The rest is the deformation CGs with mean grain size of ~1.3 μm, as presented in Fig. 2(c), high-density dislocations serves as the main deformation character. Based on TEM investigation, it is clearly demonstrated that two GNG layers sandwiching a deformation CG core structure was formed in the gage section of plate dog-bone-shaped tensile sample (denoted as GNG sample hereafter) by means of HESP, as shown in Fig. 2(d) and (e). The detailed grain size evolution along thickness from surface to center of the GNG sample was presented in Fig. 2(f).

3.2. Superb mechanical properties of the gng sample

Fig. 3 shows the mechanical properties of CG and GNG CrCoNi MEA samples. Fig. 3(a) exhibits the hardness distribution from center to surface of both samples. It is apparent that the CG sample has an uniform hardness distribution across the plate thickness, showing an average microhardness of ~322 HV. The hardness of GNG sample shows a clearly gradient distribution, reaching ~450 HV at topmost surface layer and decreased gradually to ~322 HV at center layer. Fig. 3(b) shows typical engineering stress-strain curves. The CG MEA with average grain size of ~1.3 μm (see in Fig. 1) exhibits a yield strength (0.2% offset, YS) of ~750 MPa, an ultimate tensile strength (UTS) of ~1096 MPa and remains a fracture elongation (FE) of ~41.2%, while the GNG sample processed by HESP exhibit a superior strength and ductility combination, the YS and UTS reaching up to ~1215 MPa and ~1524 MPa, respectively, meanwhile the FE remains at an remarkable value of ~23.0%. An UFG CrCoNi MEA with mean grain size of ~199 nm processed by high-pressure torsion (HPT) and subsequent annealing was presented for comparison[15], which YS, UTS and FE are ~993 MPa, ~1080 MPa and ~20.8%, respectively. Fig. 3(c) exhibits work-hardening rate curves. The strain-hardening rates of the CG and UFG MEA sample demonstrate a monotonic two-stage decrease, while that of the GNG MEA sample shows an transient increase at the ture strains range from 5% to 12%, which corresponding to the geometrically necessary dislocations (GNDs) piled up in the initial stage in HDI hardening during tensile defomation [26,31], therefore resulted in the increase of work-hardening rate, meanwhile remained a higher work-hardening rate than CG/UFG MEA. It should be noted that the uniform elongation (UE) of GNG sample is as large as 18%, while the corresponding value of UFG CrCoNi MEA is below 5%. Therefore, it could be concluded that this GNG CrCoNi MEA demonstrates a strong work hardening capacity at high-level strength.

To illustrate the superior mechanical properties of GNG sample, the comparison tensile properties (YS vs. FE, UTS vs. FE) of current work and previous reported CrCoNi and CrCoNi-based MEAs are presented in Fig. 4, and detailed information are summarized in Table 1. The comparative results clearly demonstrate that our GNG CrCoNi MEA has promising advantage in strength-ductility synergy properties. Comparing with NG CrCoNi MEA (~50 nm) processed by HPT [34], this GNG MEA shows outstanding ductility. Whilst comparing with grain refinement [7,15,32,33,35], solid solution hardening via Al/Ta [36] and $L1_2$ precipitation hardening [19] in CrCoNi MEA, this GNG sample processed by HESP bring out superior strength enhancement, exhibiting remarkable YS and UTS,

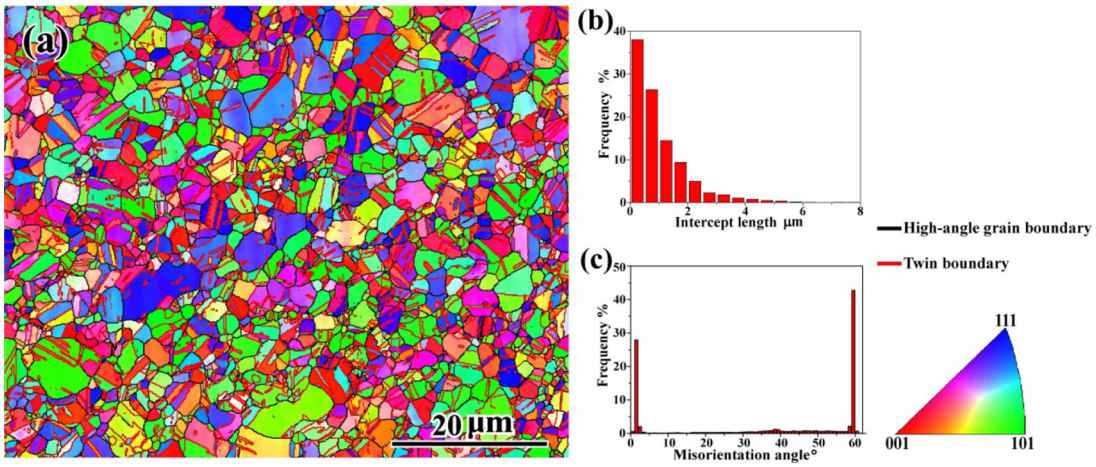

Fig. 1. EBSD investigation for CG CrCoNi MEA, (a) IPF image, (b) grain size distribution and (c) grain boundaries misorientation.

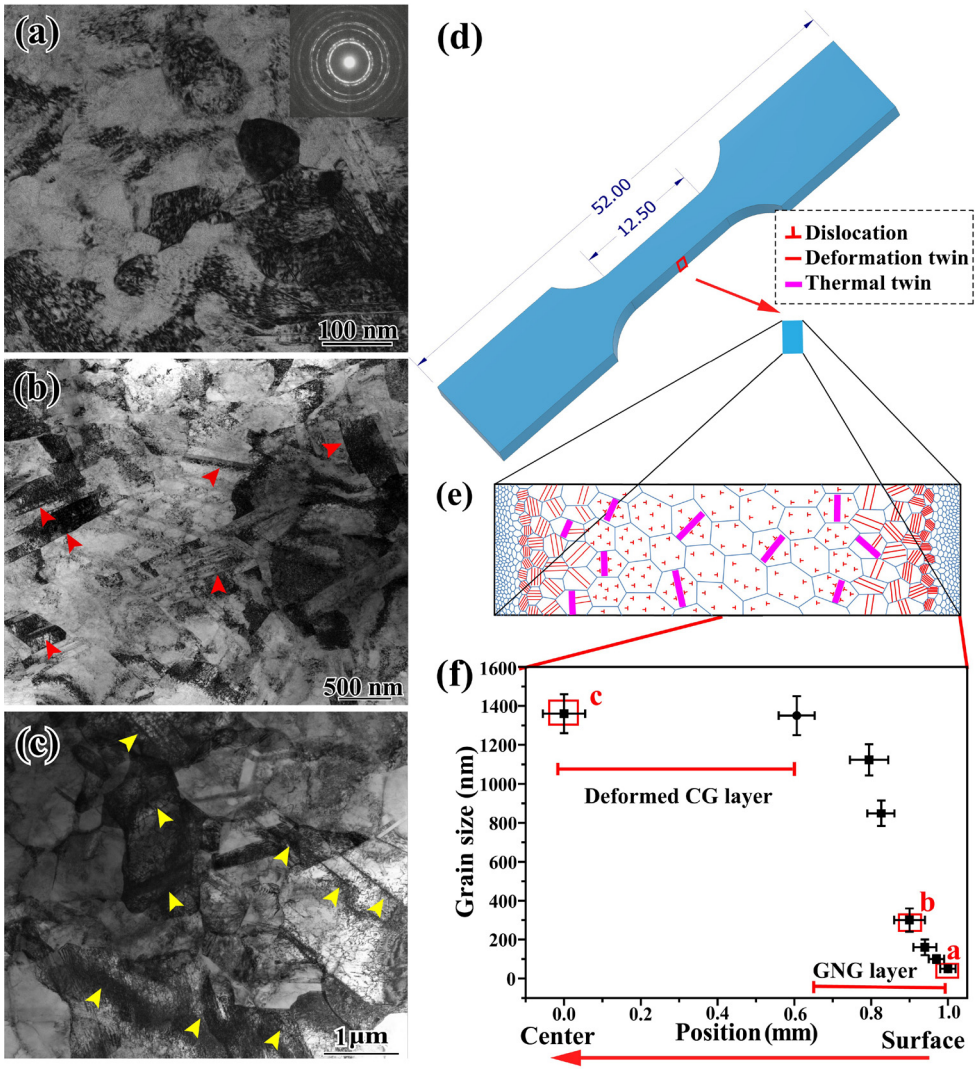

Fig. 2. Microstructure investigation for CG CrCoNi sample processed by HESP treatment, (a)-(c) representative cross-sectional TEM BF image at topmost surface, ~100 μm-deep layer and center layer, respectively, (a) NG structure, inset is the corresponding SADP, (b) twinned UFG structure, the red arrows indicate twin structure, (c) deformation CG structure, the yellow arrows indicate high-density dislocations, (d) and (e) schematic of plate tensile sample processed by HESP, showing two GNG layers sandwiching a deformation CG core, (f) average grain size distribution from center to surface layers.

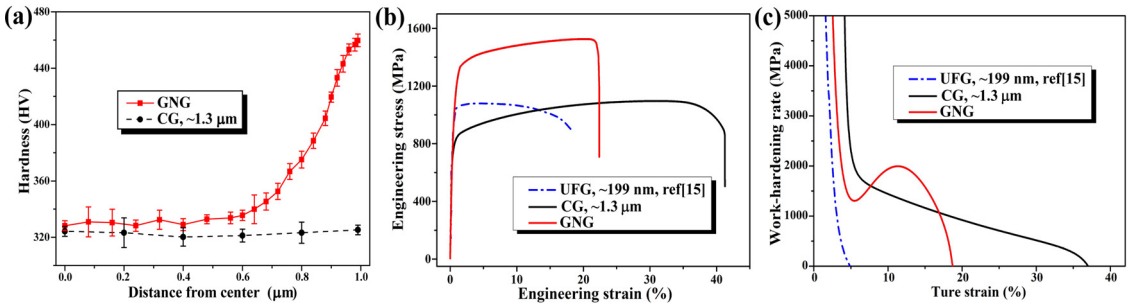

Fig. 3. Mechanical properties of CG and GNG CrCoNi MEA samples: (a) hardness distributions from surface to center, (b) typical engineering stress-strain curves, and (c) work-hardening rate curves, and the properties of an UFG CrCoNi MEA sample [15] was presented for comparison.

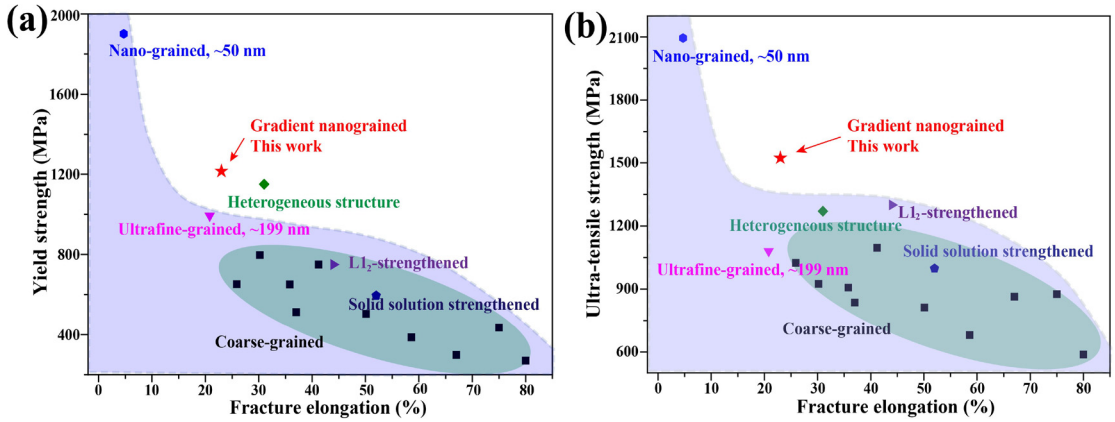

Fig. 4. The comparison results of current GNG CrCoNi MEA with previous literatures about CrCoNi and CrCoNi-based MEAs by different strengthening methods [7, 15, 19, 25, 32-36].

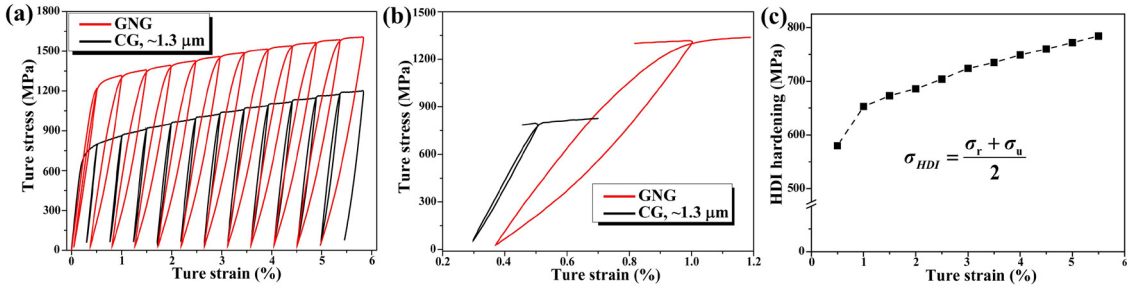

Fig. 5. (a) LUR tensile test results of CG and GNG CrCoNi MEA sample, (b) an enlarged view for comparison of hysteresis loops, and (c) calculated HDI hardening of GNG CrCoNi MEA sample, where σ_r and σ_u are reloading yield stress and unloading yield stress of an LUR loop [39].

Table 1
Alloys, processing, microstructure and tensile properties of CrCoNi and CrCoNi-based MEAs obtained from previous works and present work.

Alloys	Processing[a]	Microstructure	σ_y (MPa)	σ_{UTS} (MPa)	ε (%)	Refs.
CrCoNi	AC+1473 K/10 h/WQ+CR(80%)+973 K/1 h/WQ	FCC,GS=1.3 μm	750	1096	41.2	Present work
	AC+1473 K/10 h/WQ+ CR(80%)+973 K/1 h/WQ+HESP	FCC,GNG	1215	1524	23	
	AC+CR(90%)+1473 K/12 h/WQ	FCC,GS=111 μm	270	587	80	[15]
	AC+CR(90%)+1473 K/12 h/WQ+HPT+1173 K/20 min/WQ	FCC,GS=1.47 μm	386	680	58.6	[32]
	AC+CR(90%)+1473 K/12 h/WQ+HPT+973 K/30 min/WQ	FCC,GS=0.199 μm	993	1080	20.8	[7]
	AC+CR(92%)+1473 K/24 h/WQ+1198 K/1 h/WQ	FCC,GS=13 μm	298	863	67	[33]
	AC+1472 K/24 h/WQ+CR(60%)+1073 K/1 h	FCC,GS=~5–50 μm	435	875	75	[34]
	MA+SPS	FCC+BCC	652	1024	25.9	[25]
	AC+HPT	FCC,GS=50 nm	1901	2095	4.7	
	AC+HPT+1073 K/1 h/WQ	FCC,GS=3.3 μm	512	836	37	
	AC+1473 K/12 h/WQ+HF1323 K(90%)+CR(95%) +873 K/1 h/WQ	FCC, HGS	1150	1270	31	
	SLM	HM	651	907	35.8	[35]
$(CoCrNi)_{92}Al_6Ta_2$	AC+1498 K/24 h/WQ+CR(70%)+1423 K/3 min/WQ	FCC,GS=8 μm	595	998	52	[36]
$(CoCrNi)_{94}Al_3Ti_3$	CR(66%)+1433 K/3 min +1073 K/2 h/WQ	FCC+γ',GS=67 μm	750	1300	44	[19]

[a] AC (as-casted), CR (cold-rolled), WQ (water quenching), HESP (high energy shot peening), HPT (high-pressure torsion), MA (mechanical alloying), SPS (spark plasma sintering), HF (hot-forged), SLM (selective laser melting), GS (grain size), GNG (gradient nano-grained structure), HGS (heterogeneous structure), HM (hierarchical microstructure).

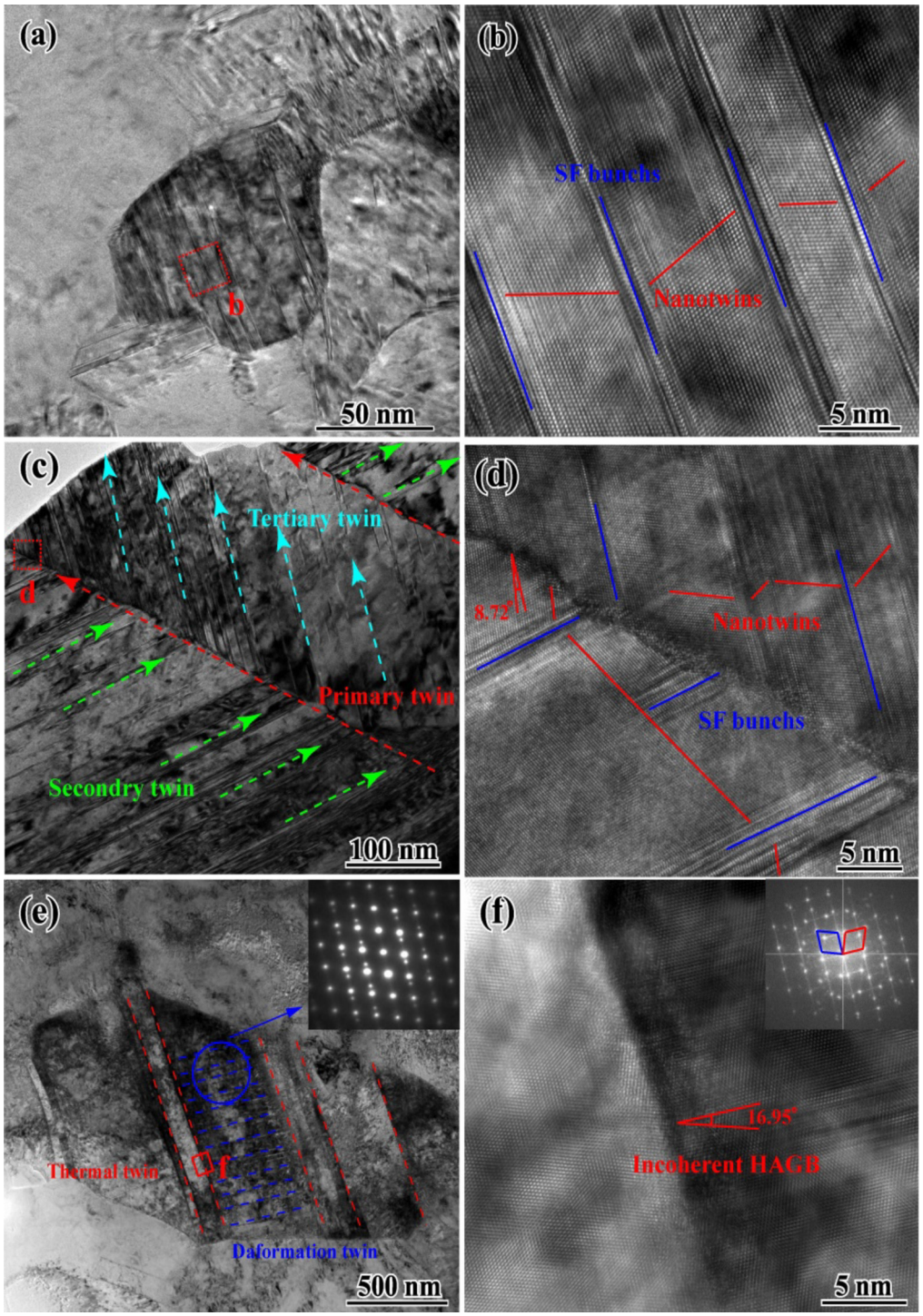

Fig. 6. Representative deformation characters in tensile tested GNG sample by TEM investigation at topest surface, ~100 μm-deep layer and center layer, respectively, (a) a deformed NG in topmost layer, (b) a HRTEM image showing deformation-induced NTs with extended SFs, (c) a deformed twinned-UFG in ~100 μm-deep layer, (d) a HRTEM image showing the enlarge view of different DTs and SFs structures, (e) a deformed CG in center layer, the inset SADP indicate the DTs structure, (d) a HRTEM image showing the thermal twin evolve into incoherent HAGB, the inset is the corresponding FFT.

as presented in Fig. 4(a) and (b), respectively. It also should be pointed out that this GNG CrCoNi MEA exhibits advantages than heterogeneous structure CrCoNi MEA processed by CR and subsequent annealing process [25], showing higher UTS and strain hardening, as shown in Fig. 4(b). Therefore, constructing GNG structure in CG CrCoNi MEA via a HESP results in high strength, excellent work hardening capacity and ductility, showing superior strength-ductility synergy properties, overcoming the longstanding strength and ductility tradeoff, which offer a strong potential for engineering application.

3.3. Reasons for superior strength and ductility synergy properties of gng samples

Based on the above microstructure investigation, the potential strengthening mechanisms of this GNG CrCoNi sample could at-

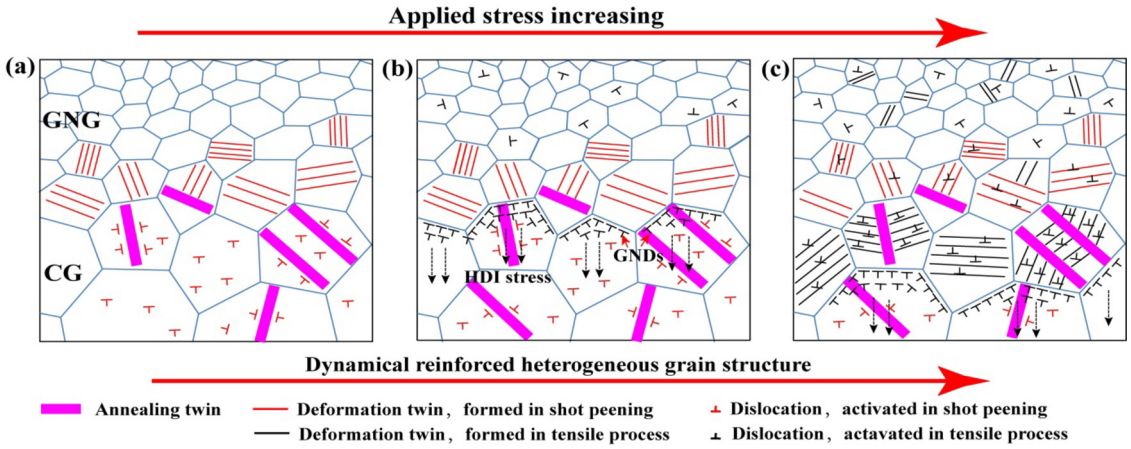

Fig. 7. Schematics of microstructure evolution in GNG sample with increasing applied stress, which exhibiting a dynamical reinforced heterogeneous grain structure during tensile process, (a) original GNG structure: (b) heterogeneous deformation results in the HDI stress in CG structure, and (c) a more heterogeneous structure forms resulting from DTs and/or SFs separating grains.

tribute to the combination of lattice friction strength (σ_0), twin strengthening ($\Delta\sigma_T$), dislocation strengthening ($\Delta\sigma_D$) and HDI strengthening ($\Delta\sigma_{HDI}$), which could be expressed as:

$$\sigma_{YS} = \sigma_0 + \Delta\sigma_T + \Delta\sigma_D + \Delta\sigma_{HDI} \quad (1)$$

where $\sigma_0 = 248$MPa, obtained from tensile result of solid-solution CrCoNi MEA [37], $\Delta\sigma_{HDI} = 643$ MPa, acquired from the LUR tests of this GNG sample (see in Fig. 5), while the combination of $\Delta\sigma_T$ and $\Delta\sigma_D$ take charge of the remainder enhancement of YS (~324 MPa), the detailed calculation process could be seen in reference [38]. Therefore, it is clearly demonstrated that the HDI hardening of this GNG sample contributes the majority of strength enhancement, leading to the extraordinary YS (~1215 MPa).

LUR test was applied on CG and GNG sample to illustrate the underlying HDI hardening effect and strain hardening mechanism, as shown in Fig. 5(a). The enlarged view of LUR hysteresis loop of those two samples is presented in Fig. 5(b). Obviously, the loop width of GNG sample is larger than that of CG sample with homogeneous grain structure, which indicate a more stronger HDI hardening effect in GNG sample[25,40,41]. Fig. 5(c) shows the evolution of HDI hardening effect of GNG sample. It is interesting to point out that HDI hardening effect of GNG sample shows an increasing trend, i.e. dynamical enhanced HDI hardening, after yielding during tensile process, which corresponding to the increasing width of LUR loops (see in Fig. 5(a)). Most important, the increase in HDI hardening contributes to the majority portion of the total stress elevation after yielding during strain hardening. The microstructural origin of the dynamical enhanced HDI hardening in this GNG sample is elaborated below.

TEM investigations were applied on the tensile tested GNG sample to reveal the domain deformation characters, as shown in Fig. 6. Different with the GNG Cu processed by SMGT [29], where grain growth of low structural stability of NG Cu contribute to the high plasticity, however in this GNG CrCoNi MEA sample no grain growth is observed, indeed DTs and/or SFs plays an critical role in microstructural evolution to sustain the excellent ductility and high strain hardening with high-level strength. For FCC-type HEAs/MEAs, because of low SFE [19,43,44], a high density of DTs and/or SFs are expected during subsequent tensile deformation. The TEM investigation indicates that the deformation-generated NGs at topmost layer in GNG sample are themselves deformable and hardenable, as presented in Fig. 6(a) and (b), deformation-induced NTs with extended SFs are observed. Fig. 6(c) and (d) shows the deformation characters in a twinned UFG at ~100 μm-deep layer, different orientations of DTs and SFs, which corresponding to the different {111} slip planes, severed as the dominate deformation characters. Fig. 6(e) and (f) presents a deformation CG at center layer of GNG sample. It is of interesting to reveal that high density dislocation accumulated at coherent thermal twin boundaries make themselves evolved into incoherent high angle grain boundaries (HAGBs) [42], which facilitate the refinement of CG. Also, numerous DTs are observed as the dominated deformation characters. In conclusion, based on the TEM investigations, high-density DTs and SFs are activated in the whole GNG sample during tensile. These DTs and/or SFs not only can hinder dislocation motion, resulting in a higher strain hardening, but also play a critical role in maintaining the heterogeneous structure in GNG sample during the whole tensile process. The heterogeneous structure was dynamically refined by high-density DTs/SFs because of the low-SFE in CrCoNi MEA, which facilitates the more heterogeneous structure after yielding during tensile process, therefore leading to the enhanced HDI hardening effect (see in Fig. 5).

The schematic structures in Fig. 7 clearly demonstrate the dynamically reinforced heterogeneous structure process in GNG sample during tensile process. For this GNG sample, see in Fig. 7(a), the deformation incompatibility of GNG layer and CG layer obviously exists caused by the difference of grain size. Comparing with CG layer, GNG layers is obvious difficult to plastically deform, therefore, due to the constraints by the still-elastic of the GNG layer, numerous GNDs generate to accommodate the stain gradient which resulted from strain incompatibility of GNG/CG layers [26,39,40,45]. The GNDs pileup results a steep strain gradient in hetreo-interfaces between GNG and CG layers, this nonhomogeneous plastic strain generates HDI stress in CG, as shown in Fig. 7(b), which makes CG layer bear more plastic deformation, i.e. more stronger, leading to significant enhancement in yield strength during tensile process [39,45-50]. Previous researches proved that HDI stress could provided effectively HDI hardening effect, produced excellent strength-ductility performance [46,51,52]. With applied stress incrasing, both GNG layer and CG layer deform plastically, as presented in Fig. 7(c). High density DTs and/or SFs are activated in the whole GNG sample caused by low-SFE of CrCoNi MEA, as revealed in Fig. 6. These numerous DTs and/or SFs result in high ductility and work hardening capacity through the following ways. First, those DTs and/or SFs can act as barriers for dislocations movement, bring considerable strain hardening effect and deformation capability. And the most importantly, those DTs and/or SFs dynamically refine the GNG sample, resulting in a more heterogeneous structure, leading to the dynamically reinforced HDI hardening effect (see in Fig. 5), which account for the majority of the

strain hardening after yielding during tensile process. Therefore, constructing GNG structure in CG CrCoNi MEA by means of HESP brings out outstanding yield strength, high work hardening capacity and excellent plasticity, showing superior strength and ductility synergy properties, which prove to be a feasible and effective way to deal with the longstanding strength and ductility tradeoff problem in FCC MEAs/HEAs, and other low-SFE materials.

4. Conclusion

In this work, a GNG structure was introduced into FCC type CrCoNi MEA through HESP treatment. The GNG CrCoNi MEA shows superior strength and ductility synergy properties, exhibiting high YS and UTS of ~1215 MPa and ~1524 MPa, respectively, remaining a good ductility of ~23.0%. HDI hardening result from heterogeneous deformation in this GNG structure contributes to the majority of the extraordinary yield strength. The dynamically reinforced heterogeneous grain structure through numerous DTs and/or SFs promotes enhanced HDI hardening effect, which help to sustain excellent ductility and strain hardening at high-level strength. Our work proves that constructing GNG structure should be a feasible and effective way to deal with the strength and ductility tradeoff problem in FCC MEAs/HEAs, and other low-SFE materials, furthermore, provides a useful insight to understanding HDI hardening in heterogeneous structure.

Acknowledgements

This work was financially supported by the National Natural Science Foundation of China (No. 51901184), the Natural Science Foundation of Shaanxi Province (2021JM-061), and the 2020 Space Science and Technology Foundation of China.

References

[1] Z. Zhang, H. Sheng, Z. Wang, B. Gludovatz, Z. Zhang, E.P. George, Q. Yu, S.X. Mao, R.O. Ritchie, Nat. Commun. 8 (2017) 14390.
[2] H.Y. Diao, R. Feng, K.A. Dahmen, P.K. Liaw, Curr. Opin. Solid State Mater. Sci. 21 (2017) 252–266.
[3] M.C. Gao, J.W. Yeh, P.K. Liaw, Y. Zhang, High-Entropy Alloys: Fundamentals and Applications, Springer, 2016.
[4] Y. Zhou, D. Zhou, X. Jin, L. Zhang, X. Du, B. Li, Sci. Rep. 8 (2018) 1–9.
[5] D.B. Miracle, O.N. Senkov, Acta Mater 122 (2017) 448–511.
[6] B. Gludovatz, A. Hohenwarter, D. Catoor, E.H. Chang, E.P. George, R.O. Ritchie, Science 345 (2014) 1153–1158.
[7] B. Gludovatz, A. Hohenwarter, K.V. Thurston, H. Bei, Z. Wu, E.P. George, R.O. Ritchie, Nat. Commun. 7 (2016) 10602.
[8] M.G. Poletti, G. Fiore, F. Gili, D. Mangherini, L. Battezzati, Mater. Des. 115 (2017) 247–254.
[9] H. Luo, S.S. Sohn, W. Lu, L. Li, X. Li, C.K. Soundararajan, W. Krieger, Z. Li, D. Raabe, Nat. Commun. 11 (2020) 3081.
[10] P. Muangtong, A. Rodchanarowan, D. Chaysuwan, N. Chanlek, R. Goodall, Corros. Sci. 172 (2020) 108740.
[11] C. Lu, L. Niu, N. Chen, K. Jin, T. Yang, P. Xiu, Y. Zhang, F. Gao, H. Bei, S. Shi, M.R. He, I.M. Robertson, W.J. Weber, L. Wang, Nat. Commun. 7 (2016) 13564.
[12] F. Granberg, K. Nordlund, M.W. Ullah, K. Jin, C. Lu, H. Bei, L.M. Wang, F. Djurabekova, W.J. Weber, Y. Zhang, Phys. Rev. Lett. 116 (2016) 135504.
[13] Y. Tong, D. Chen, B. Han, J. Wang, R. Feng, T. Yang, C. Zhao, Y.L. Zhao, W. Guo, Y. Shimizu, C.T. Liu, P.K. Liaw, K. Inoue, Y. Nagai, A. Hu, J.J. Kai, Acta Mater 165 (2019) 228–240.
[14] D.G. Kim, Y.H. Jo, J. Yang, W.M. Choi, H.S. Kim, B.J. Lee, S.S. Sohn, S. Lee, Scr. Mater. 171 (2019) 67–72.
[15] S. Yoshida, T. Bhattacharjee, Y. Bai, N. Tsuji, Scr. Mater. 134 (2017) 33–36.
[16] G. Laplanche, A. Kostka, C. Reinhart, J. Hunfeld, G. Eggeler, E.P. George, Acta Mater 128 (2017) 292–303.
[17] C.-.C. Juan, M.-.H. Tsai, C.-.W. Tsai, W.-.L. Hsu, C.-.M. Lin, S.-.K. Chen, S.-.J. Lin, J.-.W. Yeh, Mater. Lett. 184 (2016) 200–203.
[18] P. Sathiyamoorthi, J. Basu, S. Kashyap, K.G. Pradeep, R.S. Kottada, Mater. Des. 134 (2017) 426–433.
[19] Y.L. Zhao, T. Yang, Y. Tong, J. Wang, J.H. Luan, Z.B. Jiao, D. Chen, Y. Yang, A. Hu, C.T. Liu, J.J. Kai, Acta Mater 138 (2017) 72–82.
[20] W. Lu, X. Luo, Y. Yang, K. Yan, B. Huang, P. Li, Mater. Sci. Eng. A 780 (2020) 139218.
[21] W. Lu, X. Luo, Y. Yang, B. Huang, P. Li, Intermetallics 129 (2021) 107036.
[22] J.Y. He, H. Wang, H.L. Huang, X.D. Xu, M.W. Chen, Y. Wu, X.J. Liu, T.G. Nieh, K. An, Z.P. Lu, Acta Mater 102 (2016) 187–196.
[23] T. Yang, Y.L. Zhao, B.X. Cao, J.J. Kai, C.T. Liu, Scr. Mater. 183 (2020) 39–44.
[24] E. Ma, X. Wu, Nat. Commun. 10 (2019) 5623.
[25] M. Yang, D. Yan, F. Yuan, P. Jiang, E. Ma, X. Wu, Proc. Natl. Acad. Sci. USA 115 (2018) 7224–7229.
[26] Y. Zhu, X. Wu,Mater. Res. Lett. 7 (2019) 393–398.
[27] Y. Ma, F. Yuan, M. Yang, P. Jiang, E. Ma, X. Wu, Acta Mater 148 (2018) 407–418.
[28] Z. Cheng, H. Zhou, Q. Lu, H. Gao, L. Lu, Science 362 (2018) 6414.
[29] T.H. Fang, W.L. Li, N.R. Tao, K. Lu, Science 331 (2011) 1587–1590.
[30] Z. Li, K.G. Pradeep, Y. Deng, D. Raabe, C.C. Tasan, Nature 534 (2016) 227–230.
[31] Y.F. Wang, C.X. Huang, X.T. Fang, H.W. Höppel, M. Göken, Y.T. Zhu, Scr. Mater. 174 (2020) 19–23.
[32] J. Miao, C.E. Slone, T.M. Smith, C. Niu, H. Bei, M. Ghazisaeidi, G.M. Pharr, M.J. Mills, Acta Mater 132 (2017) 35–48.
[33] I. Moravcik, J. Cizek, Z. Kovacova, J. Nejezchlebova, M. Kitzmantel, E. Neubauer, I. Kubena, V. Hornik, I. Dlouhy, Mater. Sci. Eng. A 701 (2017) 370–380.
[34] B. Schuh, B. Volker, J. Todt, K.S. Kormout, N. Schell, A. Hohenwarter, Materials 11 (2018) 662.
[35] B. Han, C. Zhang, K. Feng, Z. Li, X. Zhang, Y. Shen, X. Wang, H. Kokawa, R. Li, Z. Wang, P.K. Chu, Mater. Sci. Eng. A 820 (2021) 141545.
[36] D.D. Zhang, H. Wang, J.Y. Zhang, H. Xue, G. Liu, J. Sun, J. Mater. Sci. Technol. 87 (2021) 184–195.
[37] W. Lu, X. Luo, Y. Yang, B. Huang, Mater. Chem. Phys. 251 (2020) 123073.
[38] Z. An, S. Mao, Y. Liu, H. Zhou, Y. Zhai, Z. Tian, C. Liu, Z. Zhang, X. Han, J. Mater. Sci. Technol. 92 (2021) 195–207.
[39] M. Yang, Y. Pan, F. Yuan, Y. Zhu, X. Wu, Mater. Res. Lett. 4 (2016) 145–151.
[40] X. Wu, M. Yang, F. Yuan, G. Wu, Y. Wei, X. Huang, Y. Zhu, Proc. Natl. Acad. Sci. USA 112 (2015) 14501–14505.
[41] C.W. Sinclair, G. Saada, J.D. Embury, Philos. Mag. 86 (2006) 4081–4098.
[42] Y.B. Wang, X.Z. Liao, Y.H. Zhao, E.J. Lavernia, S.P. Ringer, Z. Horita, T.G. Langdon, Y.T. Zhu, Mater. Sci. Eng. A 527 (2010) 4959–4966.
[43] S.F. Liu, Y. Wu, H.T. Wang, J.Y. He, J.B. Liu, C.X. Chen, X.J. Liu, H. Wang, Z.P. Lu, Intermetallics (2017) 1–5.
[44] Y.H. Zhang, Y. Zhuang, A. Hu, J.J. Kai, C.T. Liu, Scr. Mater. 130 (2017) 96–99.
[45] C.X. Huang, Y.F. Wang, X.L. Ma, S. Yin, H.W. Höppel, M. Göken, X.L. Wu, H.J. Gao, Y.T. Zhu, Mater. Today 21 (2018) 713–719.
[46] Z.H. Cong, N. Jia, X. Sun, Y. Ren, J. Almer, Y.D. Wang, Metall. Mater. Trans. A 40 (2009) 1383–1387.
[47] X. Wu, P. Jiang, L. Chen, F. Yuan, Y.T. Zhu, in: Proc. Natl. Acad. Sci. USA, 111, 2014, pp. 7197–7201.
[48] X. Wu, Y. Zhu, Mater. Res. Lett. 5 (2017) 527–532.
[49] X. Liu, F. Yuan, Y. Zhu, X. Wu, Scr. Mater. 150 (2018) 57–60.
[50] Y. Wang, M. Yang, X. Ma, M. Wang, K. Yin, A. Huang, C. Huang, Mater. Sci. Eng. A 727 (2018) 113–118.
[51] M.X. Yang, F.P. Yuan, Q.G. Xie, Y.D. Wang, E. Ma, X.L. Wu, Acta Mater 109 (2016) 213–222.
[52] Q. Han, A. Asgari, P.D. Hodgson, N. Stanford, Mater. Sci. Eng. A 611 (2014) 90–99.